*Landform Analysis, Vol. 21, 57–74, 2012*

# Surface NMR survey on Hansbreen Glacier, Hornsund, SW Spitsbergen (Norway)

**Valenti Turu**

*Marcel Chevalier Earth Sciences Foundation, Andorra, e-mail: vturu@andorra.ad*

**Abstract:** Glaciers are widely spread on polar and sub-polar regions but also on middle latitude mountains, where cold-dry type glaciers, polythermal glaciers and temperate-wet glaciers are respectively present. Polythermal glaciers have a cold-ice layer (temperature below the pressure melting point) overriding a temperate-ice layer. Nineteen magnetic resonance soundings were done following a 3 Km profile on Hansbreen front. Resistivity on the glacier surface, magnetic susceptibility of rocks, electromagnetic noise and total earth's magnetic field measurements confirm that the MRS survey took place in the best conditions. MRS data show different signals amplitudes at the Larmor frequency according to the loop dimension. In a very high electrical resistive context (>2 Mega Ohms meter for glacier ice) the surveyed depth is directly related to the loop area. For small loops (30 m square loop) amplitudes around 50 nV are common as well as some decay time ($T^*_2$) above 300 ms. Enlarging the loop size (60 m square loop) it is possible to observe a decrease of the signal amplitude at the Larmor frequency ($E_0 < 20$ nV) but also the time decay (100 ms >= $T^*_2$ >40 ms). Increasing loop sizes (90 and 120 m square loops), a slight increase in amplitude at the Larmor frequency, close to 30 nV, is observed with very high time decays ($T^*_2$ >500 ms). Ground Penetrating Radar surveys were carried out in Hansbreen at the same location as the MRS surveyed zone. Available GPR data show a water content of 2,5% on the cold-ice layer (the first 35 m depth) and 2% of water content on the temperate-ice layer but a 4% of water content can also be detected. Both geophysical methods are not convergent because some water content on ice has too short relaxation times being undetectable with conventional MRS devices. In that sense the low $T^*_2$ time decays data from large MRS loops elucidates that at the temperate-ice layer water flows by seepage through veins and microfractures at a very low rate toward the glacier bottom and a large amount of free water is close to the cold/temperate transition surface. In the cold-ice layer large $T^*_2$ time decays are common because water flows through fissures or karstic like conduits. In summary, combining the MRS and GPR techniques gives glaciologists a powerful toolkit to elucidate water flow-paths on glaciers, supercooled meltwater content and subglacial water or aquifers.

**Keywords:** Polythermal glacier, Surface nuclear magnetic resonance sounding (MRS), GPR (Ground Penetrating Radar), englacial water content, subglacial meltwater, subglacial aquifers, free water content.

## Introduction and objective

In occasion to the International Polar Year (2007–2009) activities a first expedition was done inside the IAG/AIG Regional Conference on Geomorpology (Kostrzewski, Zwoliński 2007), looking for candidate glaciers to carry on a surface nuclear magnetic resonance survey at 1-Elisebreen on Kaffioyra (Forlandsundet), 2-Ebbabreen on Petuniabukta (Billefjorden), 3-Scottbreen and Renardbreen on Calypsobyen (Bellsund) and finally 4-Hansbreen (Fig. 1). Hansbreen in Hornsund fjord emerged as the best site to do a large surface NMR survey for logistic reasons. Thanks to a lodging grant from the Polish Institute of Geophysics in Hornsund, from August 21th to September 10th, 2009, and the logistic support of the Wrocław University, nineteen magnetic resonance soundings (MRS) were conducted using a Numis Lite device of Iris-Instruments (Fig. 2). At the second half of September 2009 Mariusz Grabiec (Śilesian University) carried out a Ground Penetration Radar (GPR) survey in order to compare NMR and GPR results (Fig. 2). Later on a complementary field campaign has been done in September 2012 to assess the magnetic susceptibility of the rocks in Hornsund in collaboration with Dariusz Ignatiuk from the University of Silesia.

The objective of the surface nuclear magnetic resonance survey (SNMR) is to show the possibilities of the method to directly detect the water content within thermal layered type glaciers. This paper try to encourage others scientist to apply the SNMR met-

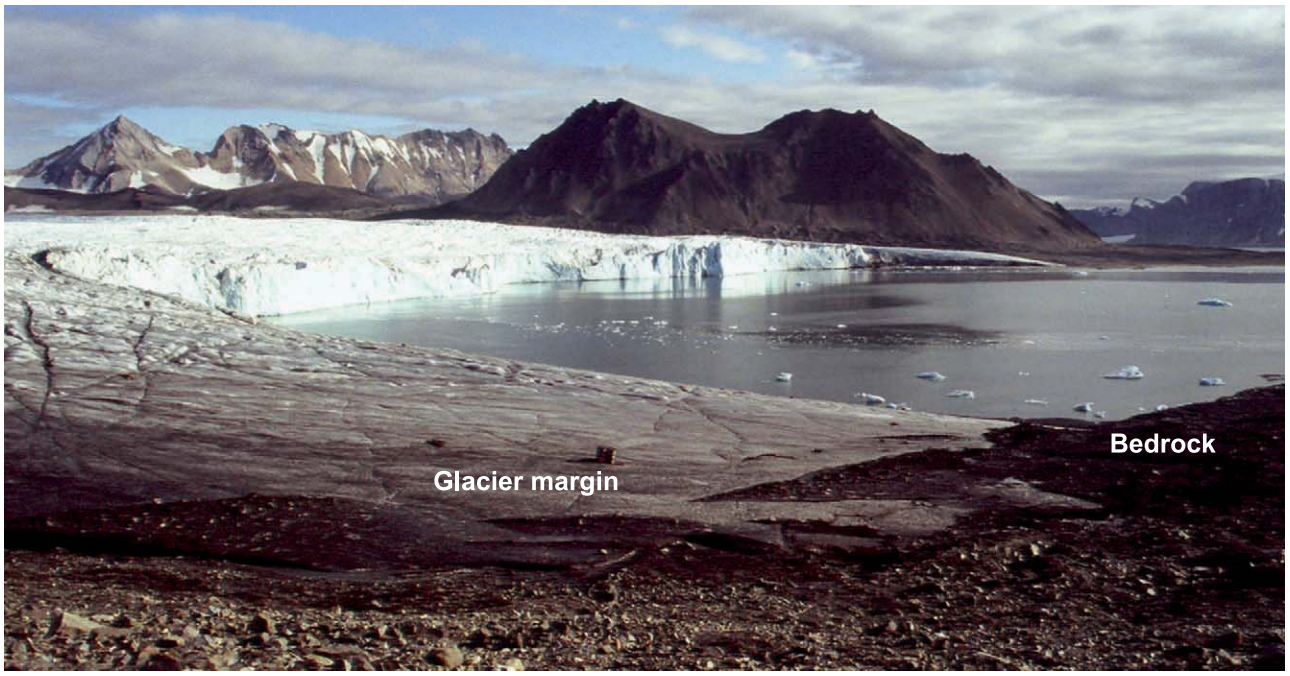


Fig. 1. Hansbreen calving ice-cliff, a tidewater grounding glacier at Siedleckivika bay on Hornsund fjord, September 2009

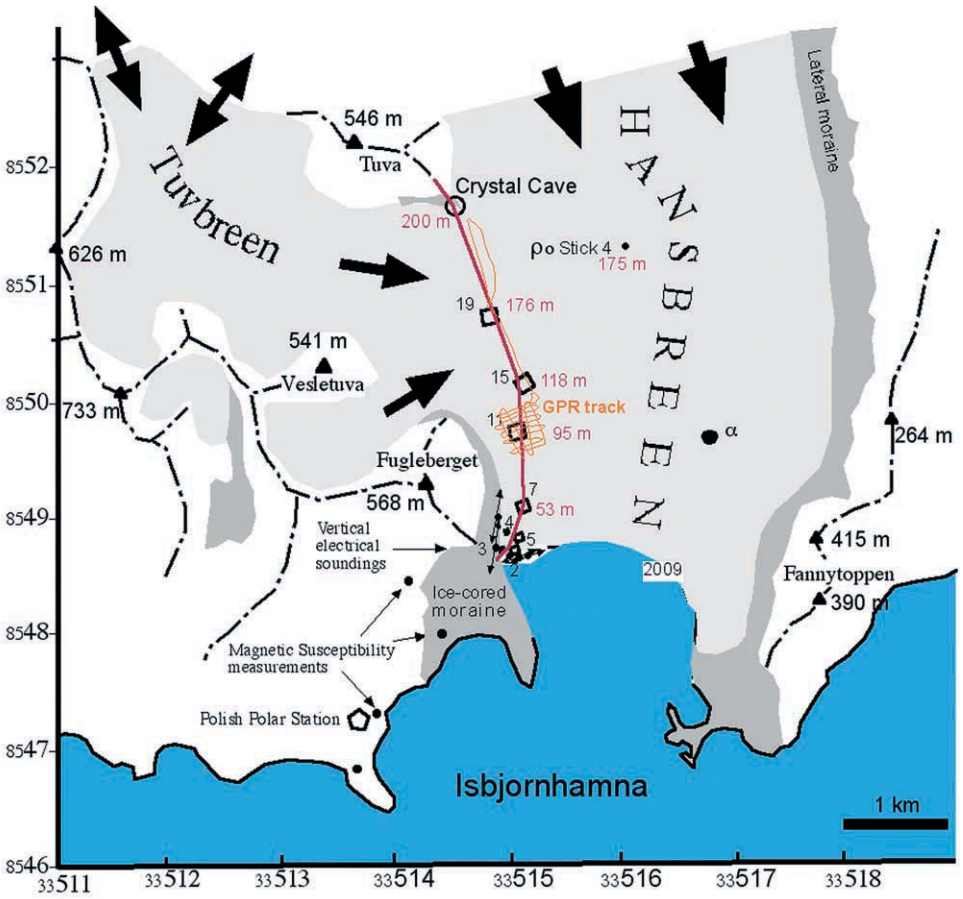


Fig. 2. The surface NMR survey has been done on the ablation zone, between the front on Siedleckivika bay (Isbjörnhamna) and Tuva mountain

On red MRS stations altitudes about see level. biggest loops (black squares) for each MRS stations are plotted as simple numbers on black. Vertical electrical soundings (VES) are drawn as small black arrows showing the electrodes wings directions. Orange brushed lines are the GPR tracks. Big black arrows indicate the main ice flow directions. Dotted black lines represents the mountain ridges and black triangles the peaks. Pentagon figure show the HRN Polish polar station location. The black round points indicate the magnetic rock susceptibility measurements. Discontinuous line, Hansbreen front in 1992 and solid line in 2009. Solid grey and light grey glacial moraines and glacier ice

hods and compare the results with those of Ground Penetration Radar (GPR), a non direct geophysical method that has become the standard method to assess the water content in glaciers, until now.

## Glaciological setting

Svalbard subpolar glaciers (Ahlmann 1935 in Jania et al., 1996) had an ice body at pressure melting point temperatures (temperate-ice layer) under a cold one (temperature below the PMP or pressure melting point). Thermal layered glaciers are quite common in the Svalbard archipelago (Pälli, 2003) and they are classified as polythermal glaciers in the sense of Fowler and Larson (1978 in Menzies, 1995a). Polythermal glaciers are also present in the Alps, Canadian Artic, Caucasus, Polar Urals and Altai (Pälli 2003) where the snout, lateral margins and surface of the glacier are below the PMP (Bennett and Glasser, 2009). Outlined for the first time in 1964 (Jania et al. 1996), Svalbard-type polythermal glaciers have the particularity that the thickness of the cold layer generally increases from the equilibrium-line altitude (ELA) down to the glacier terminus.

### Water content data from Hansbreen and internal structure

Hansbreen glacier is a medium size (56 km$^2$) tidewater glacier (the glacier front is grounded in a fjord with water level subject to tidal influence), close to it the HRN Polish Polar Station (Fig. 2) is located in the entrance of the Hornsund fjord (SW Spitsbergen). As all polythermal-type glaciers, Hansbreen has a cold-ice layer above a temperate-ice layer (Fig. 3a). The boundary between them (the cold/temperate transition surface, CTS) has been studied using borehole thermometry (Fig. 3b) and several geophysical survey methods, specially by radar (airborne UHF data and RES radar eco-sounding, CDP common-depth point radar survey and GPR ground-penetrating radar; all reported by Jania et al. 1996; Moore et al. 1999 and Pälli, 2003), which found an internal reflection horizon (IRH) close to the CTS but not necessarily coincident (Jania et al. 1996). The most important source of glacial water comes from melting due to surface ablation (Bennett & Glasser, 2009), which in Hansbreen it depends on daily mean and maximum air temperatures but also on wind speed conditions (K. Migała, com. pers. 2010). So the surface melting and runoff can dramatically change daily. Also englacial water recharges through crevasses and moulins from the cold-ice layer. Crevasses and moulins have been reported in many places on Hansbreen surface (Jania et al. 1996; Moore et al.

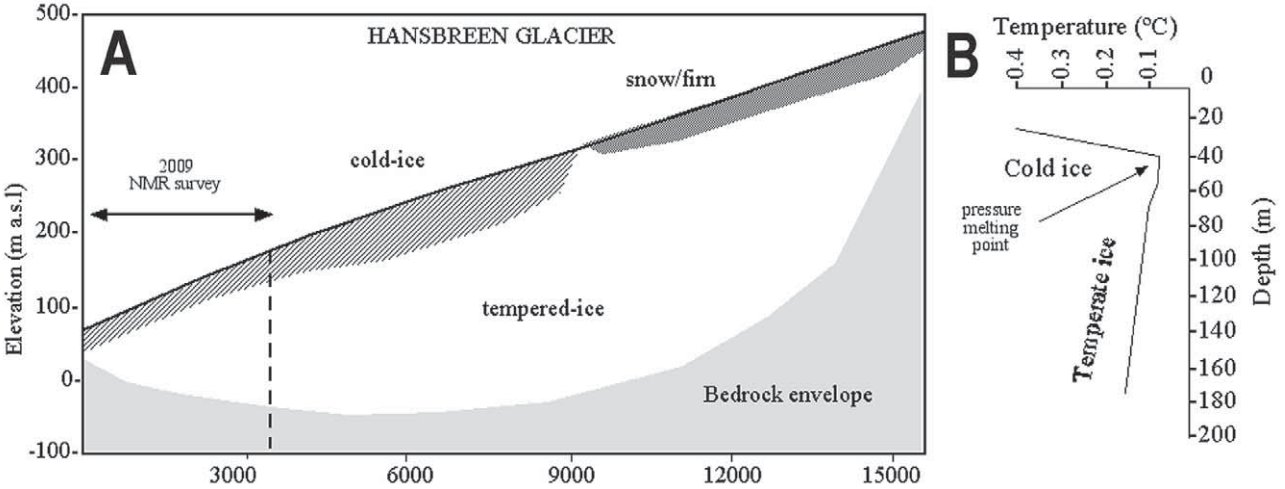


Fig. 3. A – Hansbreen polythermal-type glaciers have a layer of cold-ice in their accumulation zone and a temperate ice layer in their ablation zone (figure based on Moore et al. 1999). B – thermal profile after Jania et al. 1996

Above the ELA (equilibrium-line altitude) melted snow percolating down to through the firn layer (old ice-snow complex) to form perched water layers into crevasses; near to the end of the firn layer (on the lower half of the glacier, close to the ELA) percolating water refreezes to form superimposed ice on the surface of the glacier and wetted-refrozen snow & ice on the higher altitudes; while in the ablation zone (below the ELA) seasonal snow melts and water flows directly across the glacier surface into crevasses and moulins (Bennett and Glasser, 2009). The boundary between cold-ice and temperate layer is sensitive to variations in ice mass-balance (snow/firn accumulation or ablation) and to meltwater flowing down to the cold-ice layer (Petterson 2004). Hansbreen temperature profile (below 0æC) at its ablation zone. Two main layers form the thermal structure at the ablation zone (at a temperature measurements point, see Fig. 2), cold ice for the uppermost layer and temperate ice below (Jania et al. 1996). The increase in temperature with depth is due to the insulating effect of the overlying layer of ice and the increase in pressure with depth, until reaching the PMP tendency (pressure melting point reached here at 40 m depth). If the decrease in temperature with depth does not follow the PMP line, then the temperature on ice follows the rate at which the geothermal gradient heat is conducted away from the base of a glacier (also frictional heat produced by sliding at the glacier bottom and by internal deformation, Bennett & Glasser 2009)

1999; Bennett & Glasser 2009). Those conduits are usually viewed as complex interconnected cavities within a 3D gallery system. But in function of the glacier thermal regime, seepage system of tube-veins is also possible and has been reported by Jania et al. (1996) and Moore et al. (1999) in Hansbreen below the IRH and presumably below the CTS. In that sense micro-channels were recognized in Amundsenisen ice-cores by Zagorodnov & Zotilov (1981 in Jania et al. 1996), the thickest glacier on SW Spitsbergen with highly mineralised water (Pulina 1986 in Jania et al. 1996). This small englacial water content, which provides ice at pressure melting point such a system of small tubes and veins, can operate as seepage, but limited in flux rate. Menzies (1995b) reported a hydraulic conductivity of 9 m par year for such type of veins. Nevertheless, seepage is important in transporting meltwater, and holds the creep rate of polycrystalline ice (Duval 1977 in Menzies 1995b). Even within polar ice, such discrete liquid veins exist but separated from seepage, supercooled meltwater accumulates impurities from the solid ice and alters the pressure melting point. Jania et al. (1996) explained such a possibility in Hansbreen by the differences recorded between the measured temperature at pressure melting point and the pure liquid equilibrium temperature below the CTS.

Other sources of glacial water come from ice melting due to internal heat gradient (by geothermal source but also by internal deformation and sliding friction heat), especially close to the glacier front where the temperate-ice layer is at higher temperature than the PMP (Jania & Pulina 1990 in Jania et al. 1996). The whole hydrological system is subglacially drained by channels where meltwater flows directly to the sea (Jania & Pulina 1996 in Moore et al. 1999) following the subglacial topography (Pälli 2003). Is also noticeable that Hansbreen overlie ancient marine sediments from the last interglacial (Jania com. pers. 2009), suspected that had been frozen by sub-sea permafrost (Jania et al. 1996), overlaid by mid Holocene peat (Oerlemans et al. 2011) being the whole as a potential subglacial aquifer.

Specific GPR data has been provided for this study by Mariusz Grabiec in order to locate the IRH and the glacier bottom depth. Summarised data is shown in Table 1, enough to satisfy the objectives of the MRS survey. A general decreasing pattern for water content with depth is possible to observe in Table 1 until the CTS (Cold/Temperate transition surface). On the temperate-ice layer multiple reflections can be seen below the IRH (Internal Reflection Horizon) from Moore et al. (1999) data and also in GPR profiles from Mariusz Grabiec, showing a continuous wet-ice layer on the temperate zone.

## Method

SNMR techniques are the only geophysical procedure that detects from the surface the presence of free water in the subsurface. The way thru is using MRS procedures, by increasing gradually the excitation magnetic field in order to investigate deeper layers of the subsurface. However this technique is limited by the electrical conductivity of the subsurface, the magnetic field (inclination and magnitude), the loop antenna size, the electromagnetic noise and the presence or absence of magnetic rocks.

Table 1. Hansbreen water content from ground penetrating radar data (GPR)

| Glacial zones | Internal structures | Crystal cave | | Tuvbreen-Fuglebreen | | Steel stick | |
|---|---|---|---|---|---|---|---|
| | | Depth | w% | Depth | w% | Depth | w% |
| Cold-ice | Surface runoff | 5 m | ? | 5 | ? | 5 m | ? |
| | Crevassed zone | 20 m | 1.2–1.4 | 15 | ? | ~9 | 1.2–3.0 |
| | Englacial Channels | | | | | 15 m | ? |
| CTS? | Englacial Channels? | 60 m | 1.5–1.7 | | | | |
| CTS | | 90 m | 0.8–0.9 | 36 | 1.2–1.4 | 25 | > 1.4 |
| Temperate-ice | IRH | 110 m | > 0.9 | 53 | > 1.4 | 40 m | > 1.4 |
| Glacier bottom | Bottom refraction | 150 m | ? | 100 m | ? | 73 m | ? |
| Subglacial aquifer | Refraction structures | Subglacial material & bedrock contact | | Hyperbolic related to the glacier bottom | | Aggradation | |

Ground Penetrating Radar (GPR) main results for the upper part of the surveyed profile. Hansbreen internal structure reported from Jania et al. (1996). Water content results (w%), have been obtained from Moore et al. (1999, Table 1, Baza cave profile and Tuvbreen data). Cold/Temperate surface (CTS) and Internal refraction horizon (IRH) has been identified using GPR data (courtesy of Mariusz Grabiec, Slaski University), also the bottom of the glacier and some subglacial reflectors have been recognized. Water content on IRH interface is not known in the Tuvbreen-Fuglebreen zone and is expected to be similar to the others two sites. Water content beneath the glacier is not known but the glacier overlays soft sediments, so the presence of a subglacial aquifer is highly probable.

## MRS procedures

For a given geographical location the value of the Larmor frequency is related to the gyromagnetic ratio (g) of hydrogen protons and the total geomagnetic field ($f_L = \gamma Bo/2\Pi \approx 0{,}042577$ Bo = Bo Sin [2,442°], Bo in nT). The properties of Larmor frequency ($f_L$ in Hz) are used commonly in hydrogeology for groundwater surveying. The hydrogen protons of water molecules can be excited ($\Delta H^+$) if an electromagnetic pulse at their local Larmor frequency is transmitted from the surface using a radio-frequency transmitter. When the electromagnetic pulse (q) is removed, the absorbed energy is released and can be detected by a receiver device (a new electromagnetic field is obtained at the same frequency). A voltage (Eo amplitude) is obtained with a decaying exponentially with a constant time $T_2^*$ in a non homogeneous magnetic field (open air conditions), which at the same time is: $1/T_2^* = 1/T_1 + 1/T_2 + \gamma\Delta H^+/2$; where $T_1$ is the longitudinal constant time of the NMR signal in the z magnetic axis which is not affected by the inhomogeneities, and $T_2$ is the transversal constant time of the NMR signal in the x,y magnetic plane. In essence $T_2^* < T_2 < T_1$ but in a very low noisy environment the value of all three are very close. Decay times depend on the permeability and the initial amplitude that is directly related to the amount of water.

## MRS constrains and specific Polar and Sub-Polar constraints

Magnetism from volcanic or mineralised rocks with high magnetic susceptibility ($10^{-2}$ SI or greater) can disturb the NMR signal and cause the failure of MRS measurement, time decays ($T_2^*$ and then $T_1$) can become shorter making the groundwater undetectable in such conditions (Roy et al. 2006 in Plata & Rubio, 2007). With this regard, it is well known that the ice is not magnetic and the magnetic susceptibility measured from the surrounding rocks in the Hornsund bay is at acceptable value of $1.1*10^{-3}$ SI (Table 2, Fig. 2).

Another factor that can disturb the NMR signals is the variations of the ionosphere, which can be very strong close to the poles. Such variations influence the external component of the geomagnetic field, causing changes during the time needed to make a full MRS with the Numis system. If those variations exceed more than 250 nT (= 10 Hz) from the excitation pulse frequency resonance conditions of measuring fail. For that reason the MRS survey has been done with the automatic stacking facility from Prodiviner acquisition software (from IRIS Ltd. 2003, data acquisition software for the magnetic resonance sounding, Numis system software v03.04), which automatically sets the number of stacks needed for a given electromagnetic (EM) noise level. Because the found EM noise was very low only few stacks (16 to 82) was needed for each NMR measurement (8 to 20 pulse moments) making the data acquisition time very short (half an hour to an hour for a MRS), so in that sense the quickness of the data acquisition guaranty that the MRS has been done in an homogeneous magnetic field. However any strong magnetic field variation was reported by the HRN polar station (Table 3) during the MRS field campaign.

Since the local Larmor frequency is proportional to the intensity of the local Earth's magnetic field (Legchenko, 2007), the attenuation caused by the subsurface is greater in the poles than in the equator. However NMR signals improves the signal-to-noise ratio toward the poles because the amplitude is proportional to the square of the intensity of the geomagnetic field, which is also greater in the poles.

Thus, the best conditions are met in SW Svalbard for a MRS survey (no magnetic environ-

Table 2. Magnetic Susceptibility of the surrounding rocks from Isbjörnhamma Bay

| Rock Magnetic susceptibility | | | |
|---|---|---|---|
| X | Y | GEOLOGY | Values ($\times 10^{-3}$ SI) |
| 513691 | 8547206 | Metamorphic rock | 3.20, 2.04, 2.87, 3.16, 3.42, 3.45, 3.47 |
| 514058 | 8547411 | Metamorphic rock | 0.30, 0.60, 0.16, 0.54, 0.43, 0.46, 0.28 |
| 514872 | 8547714 | Metamorphic rock | 0.90, 0.89, 1.15, 1.45, 1.55, 1.54, 1.40 |
| 515042 | 8548309 | Moraine | 1.07, 0.51, 0.85, 0.85, 0.26, 0.21, 0.16 |
| 515070 | 8548356 | Metamorphyc rock on coast, under water during high tide | 0.88, –2.54, –1.50, –0.01, 0.14, –0.08, –0.07 |
| 514774 | 8548270 | Moraine | 0.50, 0.45, 0.62, 0.74, 0.72, 0.65, 0.72 |
| 514266 | 8548173 | Moraine | 0.78, 0.35, 0.43, 0.35, 0.68, 0.59, 0.47 |
| 514155 | 8548190 | Metamorphic rock | 2.27, 2.48, 2.26, 2.54, 2.23, 2.04, 2.13 |
| Average | | $1.11 \pm 1.09 \times 10^{-3}$ SI | |

For that propose a specific field device has been used (SM20 from GF Instruments, Brno).

Table 3. Total Earth magnetic field measurements at HRN Polish Polar Station (77°00'14"N 15°33'02"E) and the magnetic field inclination is 81°57'

| Geomagnetic field at the HRN station | | |
|---|---|---|
| Date: | Hour | Total magnetic field |
| 29/08/09 | 17H43 | 54 384 nT |
| 29/08/09 | 17H53 | 54 386 nT |
| 2/09/09 | 16H28 | 54 363 nT |
| 2/09/09 | 16H36 | 54 355 nT |
| 5/09/09 | 18H12 | 54 376 nT |
| 5/09/09 | 18H20 | 54 378 nT |
| 09/09/09 | 18H01 | 54 396 nT |
| 09/09/09 | 18H25 | 54 389 nT |
| Average | 54 378,4 ± 13,64 nT | |

ments, strong geomagnetic field by its high latitude, high impedances were reached for large loops, low electromagnetic noise and short time data acquisition).

## The mrs pilot study

Nineteen MRS were carried out in six measurement stations (Table 4, Fig. 2), for which the sizes of the square range from 900 $m^2$ to 14,400 $m^2$. The maximum current and voltage of the transmitted pulses for the small loops reached 110A and 1kV respectively. The $T_2$* and $T_1$ acquisition process performed by the MRS device was as follows: a first excitation pulse time of 40 ms, then 40 ms dead-time window imposed by the device limitations, and then a recording time window of 240 ms; immediately a second pulse moment with the same first excitation pulse

Table 4. Electromagnetic noise distribution in Hansbreen

| MRS | Latitude | Longitude | Elevation | Distance | NMR | | |
|---|---|---|---|---|---|---|---|
| | X | Y | (m a.s.l.) | (m) | Square loop ($m^2$) | Electromagnetic noise (nV) | Station |
| A | 77°00'14"N | 15°33'02"E | 2 | 260 | 3600 | 28 250 nV | Polar |
| B | 77°00'14"N | 15°33'02"E | 2 | 230 | 900 | 3 900 nV | station |
| 1 | 77°01'03"N | 15°36'22"E | 15 | 1998 | 900 (two turns) | 740 nV | Baronowski |
| 2 | 77°01'03"N | 15°36'22"E | 15 | 1998 | 3600 | 830 nV | promontory |
| 3 | 77°01'02"N | 15°36'08"E | 25 | 1968 | 900 (two turns) | 220 nV | |
| 4 | 77°01'09"N | 15°36'05"E | 43 | 2120 | 900 (two turns) | 212 nV | Siedleecki |
| 5 | 77°01'09"N | 15°36'05"E | 28 | 2149 | 3600 | 310 nV | bay |
| 6 | 77°01'13"N | 15°36'18"E | 53 | 2286 | 3600 | 180 nV | Steel |
| 7 | 77°01'13"N | 15°36'18"E | 53 | 2286 | 8100 | 460 nV | stick 1 |
| 8 | 77°01'35"N | 15°36'11"E | 95 | 2848 | 3600 | 184 nV | |
| 9 | 77°01'35"N | 15°36'11"E | 95 | 2848 | 900 (two turns) | 120 nV | Steel |
| 10 | 77°01'35"N | 15°36'11"E | 95 | 2848 | 8100 | 230 nV | stick 1b |
| 11 | 77°01'35"N | 15°36'11"E | 95 | 2848 | 14400 | 402 nV | |
| 12 | 77°01'48"N | 15°36'17"E | 118 | 3202 | 900 (two turns) | 116 nV | |
| 13 | 77°01'48"N | 15°36'17"E | 118 | 3202 | 3600 | 160 nV | Tuvabreen |
| 14 | 77°01'48"N | 15°36'17"E | 118 | 3202 | 8100 | 173 nV | Fuglebreen |
| 15 | 77°01'48"N | 15°36'17"E | 118 | 3202 | 14400 | 202 nV | |
| 16 | 77°02'11"N | 15°35'27"E | 176 | 3756 | 900 (two turns) | 205 nV | |
| 17 | 77°02'11"N | 15°35'27"E | 176 | 3756 | 3600 | 197 nV | Crystal |
| 18 | 77°02'11"N | 15°35'27"E | 176 | 3756 | 8100 | 172 nV | cave |
| 19 | 77°02'11"N | 15°35'27"E | 176 | 3756 | 14400 | 188 $\mu$V | |

Noise level equation (Y) in nano volts par $m^2$ of loop surface.
Distance (d) in meters from the noise source (HPN station)

$A = 464050; B = -2$

Location of the six NMR measurement stations and dimensions of the used loops. The electromagnetic (EM) noise detected inversely proportional to the square of the distance from the HRN polar station, so no other source of EM noise is then expected.

moment characteristics. Five electrical vertical soundings (VES) with an ABEM device (courtesy of the Faculty of Earth Sciences Silesia University) were done on the glacier margins, detecting ice cored moraines at the western margins of the glacier snout and permafrost below the sea level at the ice-cliff (Fig. 2). Two other resistivity measurements were acquired respectively at the inner part of the Hansbreen glacier (12 Mega Ohms meter for cold ice in stick 4, Fig. 2, 4) and at the front close to Baronwski peninsula (2 Mega Ohms meter for wet ice). The very high resistivity of the glacier ice exerts a beneficial role for the hardware limitation of the Numis Lite device in the high Earth's magnetic field context and large loops size, being just below the maximum capacitor configuration of the NMR device for a 120 m$^2$ loop. For small loops supplementary inductances were obtained using two cables turns configuration. However, the electromagnetic noise increased in level similar to the medium size loops.

## NMR signal and depth of investigation in Hansbreen

The NMR signal attenuation also increases inversely with the subsurface electrical resistivity. This relationship is called skin depth, and is about Zs = $(\rho_o/f_L)\hat{}(1/2)$, where $\rho_o$ is the resistivity of the subsurface and $f_L$ is the Larmor frequency. In a horizontally layered subsurface context (polythermal glacier) the measured MRS signals are limited by practically a cube of sides equal to L = 3/2 $(S)\hat{}(1/2)$, where S is the loop surface (Legchenko & Shushakov 1998). Those equations give basically the maximum reliable depth of water detection by MRS and the cube is the approximate investigated volume. On the other hand, NMR signal depth sensitivity depends on the MRS-Kernel, a non linear function involved in the stepwise inversion of MRS data (Legchenko & Shushakov 1998, Hertrich 2008), in which the loop size, Larmor frequency and the electrical resistivity structure of the subsoil is involved. In a non homogeneous medium the MRS Kernel should be computed repeatedly for each electrical resistivity (Behroozmand et al. 2012), but in polythermal glaciers does not affect the MRS Kernel significantly by its high resistivity in all type of ice.

The sensitivity function has been plotted (Fig. 5) for the Hansbreen conditions. The skin depth is greater than the biggest investigated cube because the resistivity of the glacier is really high and the hardware limitations of the Numis Lite do not permit loops greater than 14,400 m$^2$, so the maximum investigated

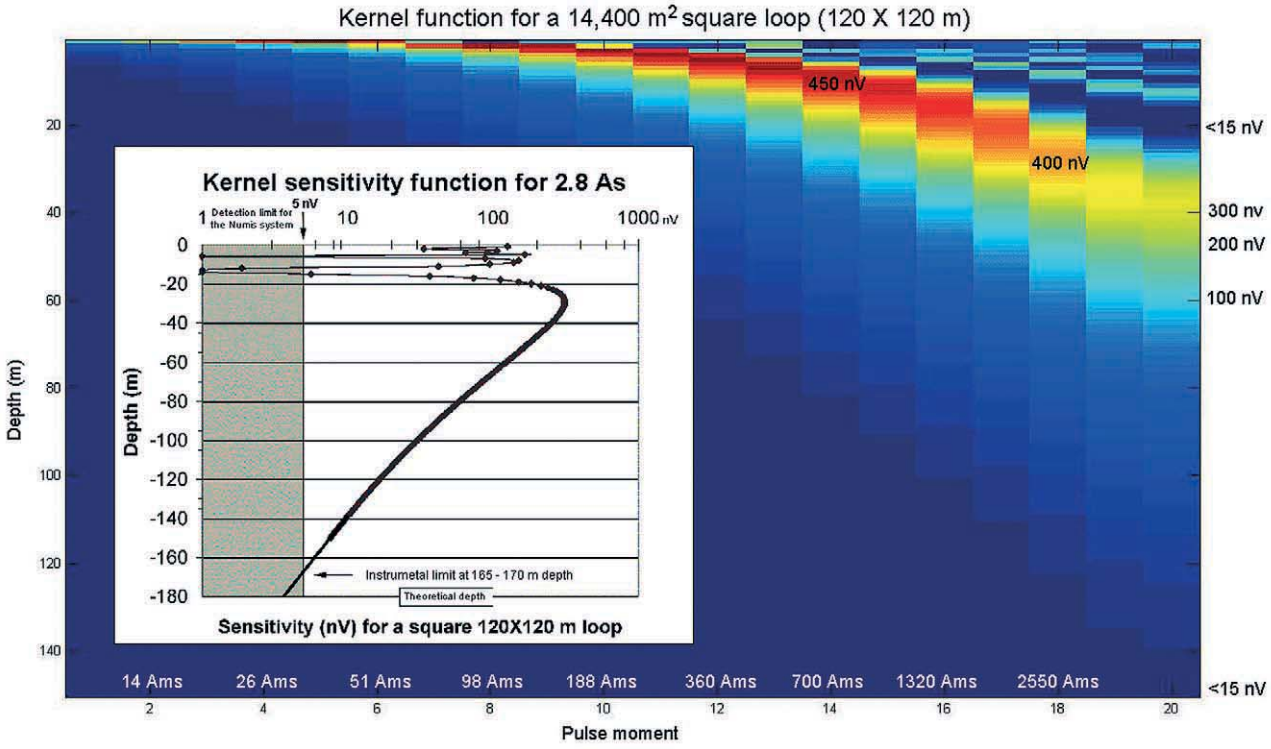


Fig. 4. Hansbreen Kernel function plotted for a 14,400 m$^2$ square loop in an ultra-high resistivity medium (2 Mega Ohms meter) with a strong Earth magnetic field (53,378 nT) and a very steep magnetic vector (81°57"), (courtesy of Rafik Soltani from the University of Petroleum from Beijing, China) using the MRSMatlab Software (from the Leibniz-Institue for Applied Geophysics). The Kernel function has been calculated for a maximum pulse moment (number 20) of 4 As, but the maximum pulse moment reached in this SNMR survey is about 2.8 As for the largest square loop (120 × 120 m). Since the instrumental detection limits of the Numis system is 5 nV the maximum sensitivity depth reached (165–170 m) with the largest loop in Hansbreen is close to the theoretical depth (L = 180 m) of the investigated cube

Fig. 5. Ice resistivity measurements (ABEM 4000 device) on stick number 4 at 175 m a.s.l. and image of the used device Numis Lite 005 at the glacier front (30 m a.s.l). Ice is a perfect electrical insulator so the maximum MRS depth is obtained by the loop size and configuration (Photo: O.Hengesch)

depth is close to 167 m limited by the instrument sensitivity (5 nV).

## MRS data from Hansbreen

The transmitter of the NMR device creates a current ($I_0$) at the Larmor frequency ($f_L$) through the loop antenna during a given time ($\tau$), creating the excitation field expressed by the pulse moment: $q = I_0\tau$ which governs the investigation depth. For each moment the amplitude ($E_0$) of the NMR signal and the decay time ($T^*_2$) has been calculated by a family of stacked values using the specific Samogon 4.041 software from Legchenko (2001) provided with the Numis Lite device. The international units system for the pulse moment is Amps par second or millisecond (As or Ams) and can be increased by increasing the intensity ($I_0$), the pulse duration ($\tau$) or both, however the pulse duration must be shorter than the relaxation time ($T_2^*$), being it geological dependent. The maximum current ($I_0$) depends on the maximum voltage (V) of the device and the loop impedance (Z) by:

$$I_0 = V / Z$$

where:

$$Z = (R^2 + L^2\omega_L^2)^{1/2}.$$

R and L being the resistance and the inductance of the loop respectively, while $\omega_L$ is $\gamma B_0$ (the hydrogen protons gyromagnetic ratio times the geomagnetic total field). Note that the impedance is mainly given by the inductance factor and it is geographically-dependent (Bernard 2007). In essence for a given site the Larmor frequency can be considered more or less constant. Deviations of no more than 10 Hz around the Larmor frequency can be considered acceptable in order to compare different magnetic resonance soundings (MRSs) at the same location. Assuming that the resistivity of the subsurface is similar for different MRSs at the same site, the differences of the pulse moment will be a function only of the geometry, form and perimeter of the loops, which can be summarised by a geometric variable: the loop area. For small loops a single cable turn or a double one has no major effect on the current because the device will also modify the voltage inversely proportionally to the impedance of the loop. Formally the pulse moment can also be written as:

$$q = V\tau / Z$$

and then:

$$qZ = V\tau$$

since $Z \sim S$, where S is the loop surface then:

$$qS \sim V\tau.$$

It means that data from different magnetic resonance soundings might be plotted together regardless of their geometry, but not only in function of the pulse moment but also proportionally to the loop surface.

Table 5. Synthetics magnetic resonance soundings (SMRS)

| Synthetic magnetic resonance sounding for Crystal cave site | | | | | | | | Table 5a | |
|---|---|---|---|---|---|---|---|---|---|
| n | MRS | L | q | q * S | $E_0$ | $T_2$* | Frequency | Phase | Noise |
| 1 | 16 | 30 | 0.502 | 451.8 | 19.72 | 1000 | 2311.26 | 82 | 6.8 |
| 2 | 18 | 90 | 0.118 | 955.8 | 24.2 | 1000 | 2310.72 | 9 | 11.5 |
| 3 | 18 | 90 | 0.154 | 1247.8 | 16.07 | 94 | 2326.36 | 168 | 7.7 |
| 4 | 19 | 120 | 0.102 | 1468.8 | 28.25 | 163 | 2311.05 | 78 | 11.3 |
| 5 | 19 | 120 | 0.132 | 1900.8 | 24.63 | 1000 | 2312.41 | 4 | 12.3 |
| 6 | 17 | 60 | 0.810 | 2916 | 22.51 | 183 | 2312.48 | 188 | 10.7 |
| 7 | 19 | 120 | 0.441 | 63450.2 | 14.33 | 671 | 2313.3 | 312 | 6.9 |
| 8 | 18 | 90 | 1.254 | 10154.4 | 52.37 | 110 | 2318.93 | 335 | 9.5 |
| 9 | 18 | 90 | 2.205 | 17860.5 | 23.59 | 107 | 2314.81 | 34 | 10.4 |
| 10 | 19 | 120 | 1.499 | 21585.6 | 29.79 | 91 | 2318.29 | 81 | 14.7 |
| 11 | 18 | 90 | 2.604 | 21092.4 | 51.79 | 20 | 2323.05 | 12 | 5 |
| 12 | 19 | 120 | 1.499 | 21585.6 | 29.79 | 91 | 2318.29 | 81 | 14.7 |
| 13 | 18 | 90 | 3.102 | 25126.2 | 12.28 | 1000 | 2310.47 | 106 | 5.9 |
| 14 | 18 | 90 | 3.382 | 27394.2 | 16.47 | 112 | 2311.08 | 350 | 4.2 |
| Units | | m | As | (As * $m^2$) | nV | ms | Hz | ° | nV |
| Synthetic magnetic resonance sounding for Fuglebreen-Tuvbreen site | | | | | | | | Table 5b | |
| n | MRS | L | q | q * S | $E_0$ | $T_2$* | Frequency | Phase | Noise |
| 1 | 12 | 30 | 0.252 | 226.8 | 31.26 | 10 | 2327.48 | 218 | 10.8 |
| 2 | 14 | 90 | 0.1168 | 946.08 | 25.58 | 161 | 2313.03 | 27 | 8.5 |
| 3 | 12 | 30 | 1.342 | 1207.8 | 18.23 | 165 | 2319 | 99 | 8 |
| 4 | 14 | 60 | 0.2844 | 2303.64 | 17.25 | 251 | 2325.1 | 180 | 6.5 |
| 5 | 15 | 120 | 0.1924 | 2770.56 | 19.81 | 1000 | 2312.05 | 6 | 7.3 |
| 06 | 15 | 120 | 0.3476 | 5005.44 | 14.59 | 1000 | 2320.49 | 182 | 7.5 |
| 7 | 15 | 120 | 0.4244 | 6111.36 | 10.72 | 1000 | 2316.77 | 86 | 5.4 |
| 8 | 15 | 120 | 1.3672 | 19687.68 | 23.8 | 180 | 2318.84 | 106 | 5.3 |
| 9 | 15 | 120 | 2.5957 | 37378.224 | 29.1 | 154 | 2314.4 | 10 | 5 |
| Units | | m | As | (As * $m^2$) | nV | ms | Hz | ° | nV |
| Synthetic magnetic resonance sounding for Steel stick site | | | | | | | | Table 5c | |
| n | MRS | L | q | q * S | $E_0$ | $T_2$* | Frequency | Phase | Noise |
| 1 | 8 | 60 | 0.250 | 900 | 21.64 | 331 | 2311.71 | 210 | 5.8 |
| 2 | 11 | 120 | 0.1332 | 1918.08 | 26.32 | 151 | 2312.51 | 333 | 8.7 |
| 3 | 10 | 90 | 0.3608 | 2922.48 | 18.62 | 70 | 2315.5 | 31 | 8.3 |
| 4 | 11 | 120 | 0.9288 | 13374.72 | 19.23 | 265 | 2312.29 | 264 | 9.5 |
| 5 | 10 | 90 | 3.3724 | 27316.44 | 11.16 | 532 | 2318.98 | 169 | 5.8 |
| Units | | m | As | (As * $m^2$) | nV | ms | Hz | ° | nV |

The presented data are from the three sites. The threshold of the device is 5 nV and according to Legchenko (2007) the signal must be two times greater than the stacked noise to be considered a water signal. The detected frequency is around the Larmor frequency (2317.1 – 2315.9 Hz) and a bias no more than 10 Hz (2327.1 Hz – 2305.9 Hz). The most robust data is the amplitude, $T_2$* is more affected by the stacking procedure for weak water signals (specially the weighted average stacking from the Prodiviner software, Juan Plata com. pers.; Rafik Soltani com. pers.) and shouldn't be interpreted as a long time decay rather that a limitation of the acquisition software of the Numis System. The phase value (between 0 and 360°) is used to have information about the resistivity changes in the subsurface but also about the sounding quality and how much the electromagnetic noise affect the signal, but such information is not necessary true for a synthetic sounding, nevertheless if we look at the MRS 19 (Table 5a) is possible to see that most of its values are close to the 81° to 78° and similar thing happen with the MRS 18 (Table 5a) but for values between the first and the fourth quadrant (335° to 12°) in a wind rose diagram type.

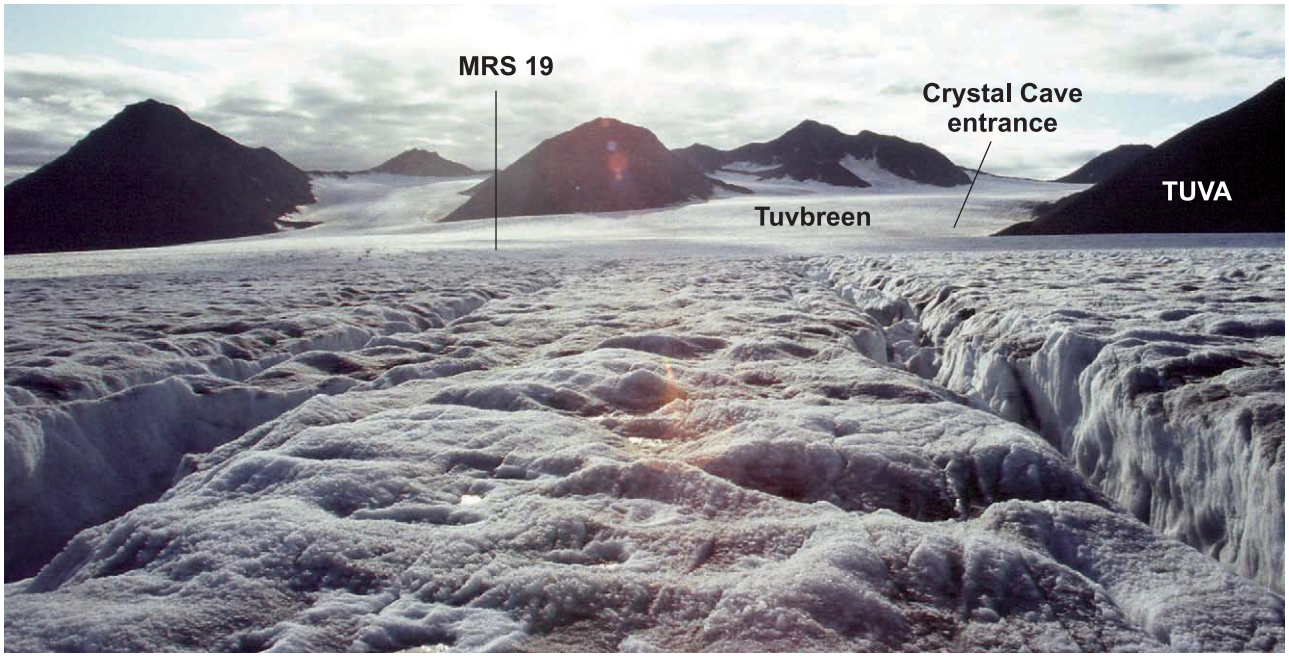


Fig. 6. Image from stick 4 (meteorological station), long open and deep crevasses on the glacier surface. The MRS survey site and Crystal cave entrance at 200 m a.s.l are both located there. Tuvbreen ice stream is in front and intersects the Hansbreen ice stream at Crystal cave

Table 5 shows the stacked data obtained at the upper part of the surveyed glacier following the quality criteria of Legchenko (2007) regardless to the signal/noise ratios. Here for each measuring station four square loops of different size were done (L = 30, 60, 90 and 120 m) reaching the sensitivity device limit of 40 m, 81 m, 122 m and 168 m on ice respectively according to the Kernel function. The lower part of the investigated area has not been conducted using large loop, given such data is not relevant for the proposal of this paper.

For Crystal cave site (176 m a.s.l, Fig. 6) the maximum amplitude values is close to 52 nV with short decay times in the central part of the synthetic sounding (Table 5a). Above such relatively high values the data range is between 14 nV and 28 nV but high oscillations in decay times are observed. Toward the bottom of the synthetic sounding the amplitude values are between 30 nV and 16 nV and some oscillations on the decay times also occur. For Fuglebreen-Tuvbreen site (118 m a.s.l.) amplitude values ranged between 10 nV and 31 nV (Table 5b), while at Steel stick site (85 m a.s.l) amplitude values ranged between 26 nV and 8 nV (Table 5c). On both sites oscillations on the decay times also occurred. Decrease pattern in amplitude signals downward from Crystal cave site are detected and show that the hydrogeological system is water-target on top of the surveyed profile.

## MRS inversion and modelling

Following the GPR data from Table 1, has been possible to calculate the expected MRS signals using Samogon software for MRS signals. Once the thermal structure of Hansbreen is known, the equivalence problem (see Legchenko and Shushakov, 1998) between water thickness and water content in ice is minimised. Also, from Table 1 general patterns on time decay are possible to correlate with the known Hansbreen hydrogeological and thermal structure. Firstly, for the surface and subsurface runoff (if not frozen) large time decays can be expected, and also for the cold-ice crevassed zone, but not near to the CTS or below the IRH zone. Secondly, toward the ice bottom and subglacial aquifer, large time decays can again be expected regarding the geological nature beneath the glacier. The 1D models for each studied site are presented on Table 6 and plotted in Fig. 7a to 7c.

Crystal cave site: From Figure 7a, two relatively high values of Eo arise from the englacial drainage system on the cold-ice layer (Fig. 8a). Before reaching those relatively high values, some MRS water signals from shallow crevasses (no more than 23 m depth) were detected. A steep dropping curve is present after those relatively high values. The model acts as an envelope of the maximum possible water content on the temperate-ice layer. The model has a final asymptotic tendency to 10 nV (twice the device threshold, 5 nV), which is compatible with the presence of a subglacial aquifer at that depth greater than 150 m. But no MRS signal was detected at such

Table 6. Synthetic Magnetic resonance sounding models

| MRS models | | | | |
|---|---|---|---|---|
| Pulse moments | Pulse moment par square loop | Crystal cave | Tuvbreen-Fuglebreen | Steel stick |
| q | q * S | Model Cc15e | Model T10f | Model Ss8d |
| 0.00 | 132.16 | 5.59 | 26.15 | 3.62 |
| 0.01 | 194.88 | 8.10 | 31.06 | 5.29 |
| 0.02 | 286.72 | 11.64 | 30.39 | 7.67 |
| 0.03 | 418.88 | 16.40 | 23.95 | 11.02 |
| 0.04 | 613.76 | 22.08 | 20.22 | 15.53 |
| 0.06 | 898.24 | 27.21 | 23.80 | 20.92 |
| 0.09 | 1314.88 | 28.50 | 20.35 | 25.63 |
| 0.13 | 1924.16 | 25.05 | 15.14 | 25.69 |
| 0.19 | 2813.44 | 27.99 | 19.87 | 17.59 |
| 0.28 | 4117.12 | 40.34 | 19.35 | 12.06 |
| 0.42 | 6021.12 | 46.56 | 13.63 | 17.84 |
| 0.61 | 8807.68 | 49.67 | 17.25 | 20.25 |
| 0.89 | 12884.48 | 53.19 | 20.96 | 18.89 |
| 1.31 | 18845.12 | 49.79 | 24.58 | 14.57 |
| 1.91 | 27565.44 | 19.29 | 25.64 | 11.08 |
| 2.80 | 40320.00 | 13.66 | 29.46 | 13.10 |
| As | As * $m^2$ | nV | nV | nV |

MRS models for Steel stick, Tuvbreen-Fuglebreen and Crystal cave sites adapting the water content data and the hydrogeological boundaries from Table 1 to the MRS data present in Table 5. The pulse moment distribution for the models were calculated using the Phar Lap's software 7.0, provided with the Numis Lite device, for a $q_{max}$ = 2.8 As and a length of 120 m for the side for a theoretical square loop of 14,400 $m^2$, in order to compare modelled data and field data.

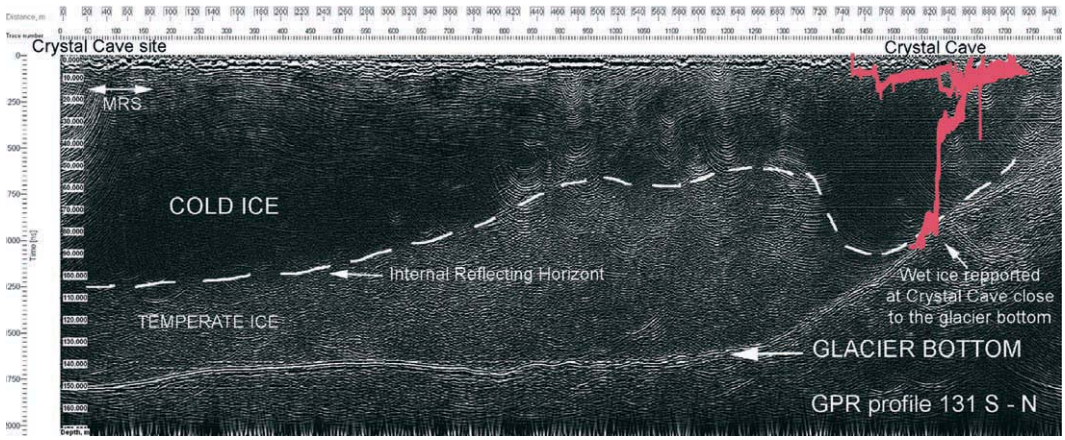


Fig. 7. GPR profiles (courtesy of Mariusz Grabiec in 2010) between Crystal cave and Steel Stick site (see Fig. 2). The superficial reflections are due to terrain irregularities and the presence of superficial and mid englacial water conduits. When a crevasse opens on the glacier surface intersects the supraglacial meltwater streams which will feed the crevasse, the water level rises until the crevasse deepens enough to intersect englacial drainage passages; the heat carried into it by the meltwater can keep the drainage passage open even when the glacier flow drive to a crevasse is closing and thereby forming a moulin

Fig. 7a. Crystal cave (plotted in red on the GPR profile) is located at the confluence between Tuvbreen and Hansbreen ice streams near to Tuva mountain at the end of the surveyed profile (see Fig. 2). Here vertical shafts were followed through more than 70 m to subglacial conduit and deep hydrofracturing occurred at this site due to a combination of extensional ice flow and abundant surface meltwater at a glacier confluence. The presence of wet ice close to the glacier bottom has been reported by Benn et al. (2009), so the surface-to-bed drainage can occur wherever high meltwater supply coincides with large ice tensile stresses

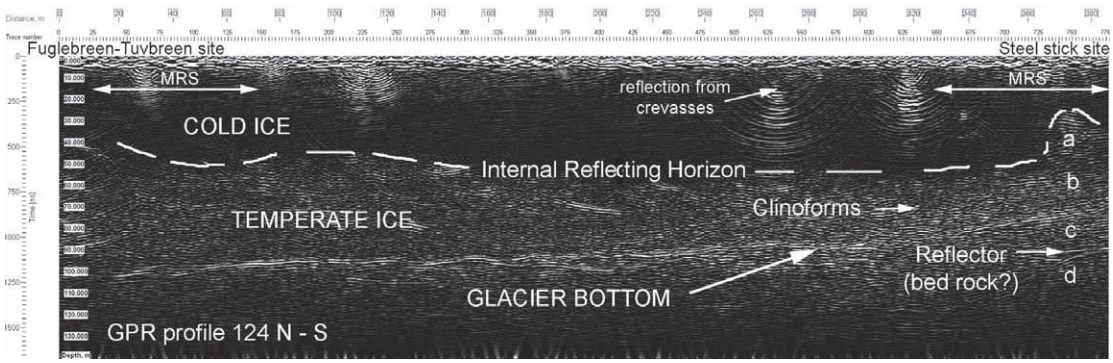


Fig. 7b. GPR profile between Fuglebreen-Tuvabreen MRS site and Steel Stick MRS station (see Fig. 2). Under the Steel Stick site a, b, c and d reflection bodies has been recognised corresponding to the CTS (a), the IRH and the temperate ice (b) with clinoforms corresponding probably to sills, the glacier bottom (c) with also clinoforms coming probably by sediments, and finally an horizontal reflector interpreted as the basement rock. Under the Fuglebreen-Tuvabreen MRS site CTS can be observed by GPR data between 30 and 40 m depth and the presence of the temperate ice below 50 m depth, glacier bottom close to 100 m depth

a depth, certainly due to a lack of stacking (Legchenko com. pers. 2009). Nevertheless, Benn & Glasser (2009) suggest that the englacial water conduits are linked to the subglacial drainage system at Crystal cave. So the model envelope in Fig. 7a should be considered the maximum water content on Hansbreen.

Tuvbreen-Fuglebreen site: The ending magnetic resonance sounding data in Figure 7b shows two remarkable values for Eo. The last one linked with subglacial features from Table 1 and Figure 8b. Here, the subglacial water has been detected and equivalences occur between the water content, the decay time and thickness. In that sense, the plotted model in Figure 7b is also possible by 20 cm of water film (w=100% and $T^*_2$>1000 ms), but also by 1 m of subglacial channel (w=22% and $T^*_2$=500 ms) or even by 5 m of subglacial aquifer of soft sediments (w=5% and $T^*_2$ = 250 ms). However, the observed hyperbolic refractions at the temperate-ice layer bottom (Table 1) suggest the presence of free water beneath the glacier, probably meltwater in subglacial linked-cavities (Kamb, 1987 in Menzies 1995, pag. 190), typically from a surging glacier. The penultimate MRS recorded point corresponds to the IRH boundary at 50 m depth (Table 1, Fig. 8b) and the cold/temperate surface at 36 m depth (Table 1, Fig. 8b) has a low water content related to the lowest amplitude data point. Cold-ice crevassing and moulins are present at

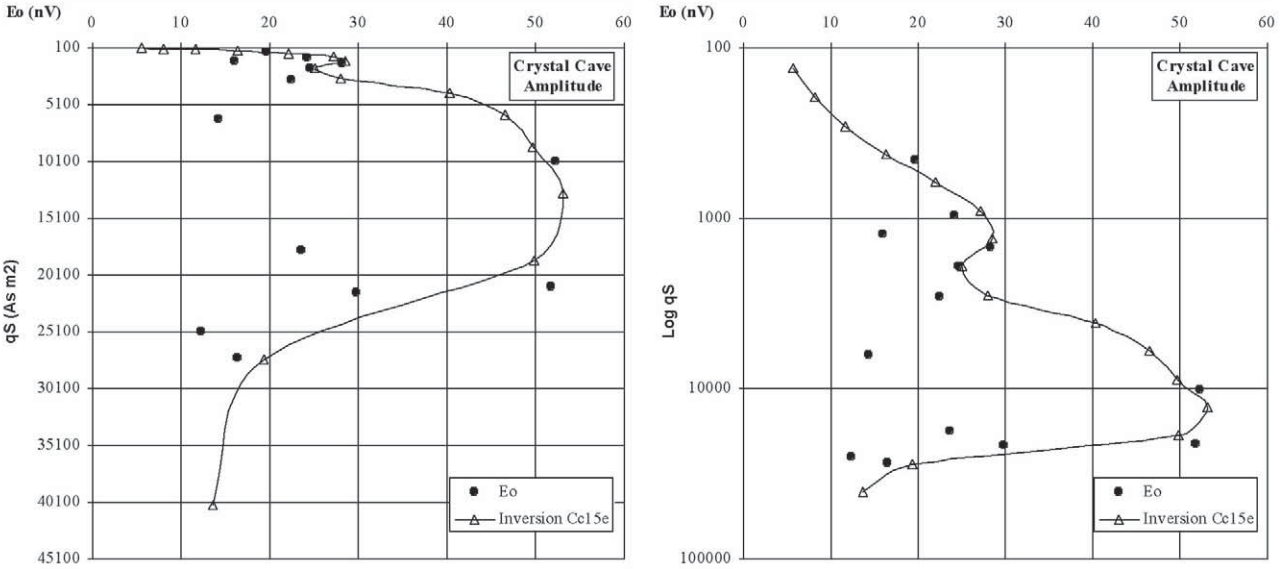


Fig. 8. Here MRS recorded data signals from Table 5 and inverted models from Table 6 have been linearly and logarithmically plotted (qS = moment per loop surface in Amps per second and square metres, Eo = Stacked amplitude in nV)

Fig. 8a. Model for Crystal cave site data from Table 5a and model from Table 6: superficial features and runoff w= 1,2% and $T^*_2$ = 510 ms between 3.5 and 7 m depth; cold-ice crevassed zone 1.5% < w <= 1.6% at 21–23,5 m depth and 46–60,1 m depth respectively (250 ms < $T^*_2$ <= 400 ms); temperate/cold-ice transition (CTS) with w=0.7% and $T^*_2$ = 90 ms between 90 and 92.5 m depth; temperate-ice layer and IRH boundary with w=0.7% and $T^*_2$ = 80 ms between 110 and 120 m depth; glacier bottom with w= 1% and $T^*_2$ = 500 ms between 150 and 152 m depth; subglacial aquifer w = 1% and $T^*_2$ = 300 ms between 152 and 170 m depth

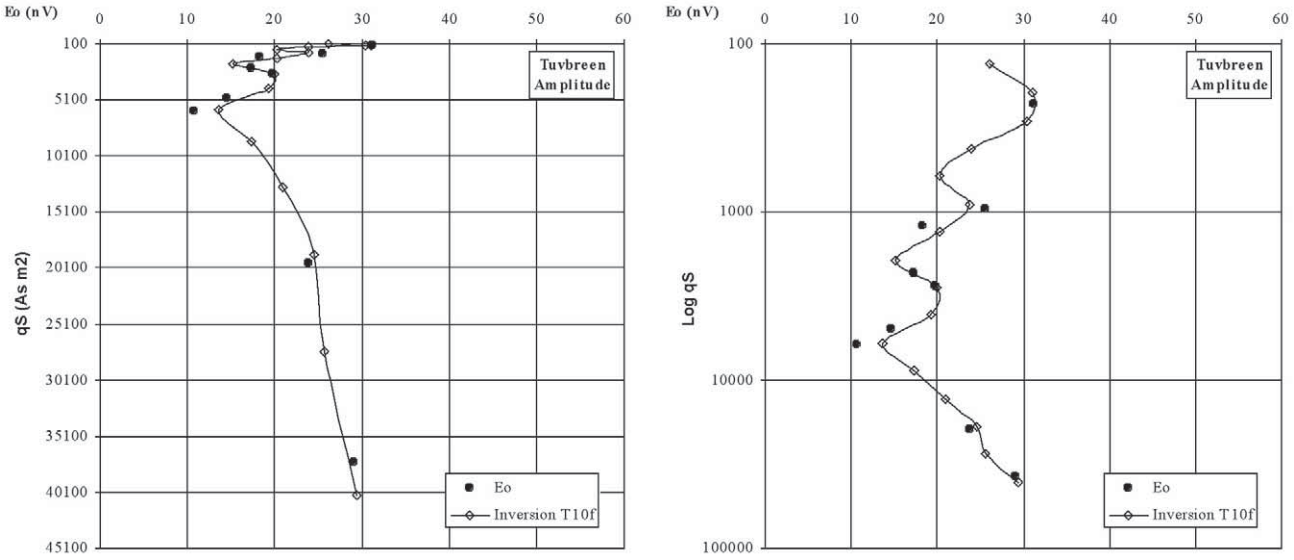


Fig. 8b. Tuvbreen-Fuglebreen site data from Table 5b and model from Table 6: Superficial features and runoff with 3% =< w < 5% and 200 < $T^*_2$ =< 510 ms between 0.5–1.6 m depth and 3–4 m depth; cold-ice crevassed zone with w=1.8% and 350 ms between 13.5–15.1 m depth, CTS transition zone at 36–36.5 m depth with w=1.25% and $T^*_2$ = 90 ms; temperate-ice layer and IRH boundary with w= 0.8% and $T^*_2$ = 90 ms between 50–52 m depth; glacier bottom with w=1% and $T^*_2$ = 500 ms between 95–98 m depth; subglacial aquifer w = 1.2% and $T^*_2$ = 200 ms between 98–120 m depth

shallow depth (< 20 m). High water volumes from superficial runoff are expected on model, up to a 4%.

Steel stick site: The last Eo magnetic resonance sounding data point in Figure 7c is linked to the subglacial drainage (Table 1, Fig. 8b). Here, the subglacial water has been detected and equivalences between water content, decay time and thickness happen as at the Tuvbreen-Fuglebreen site (Fig. 7b). In that sense, the plotted model in Figure 7c is also possible by 7 cm of water film (w=100% and $T^*_2$>1000 ms), also by 1/2 m of subglacial channel (w=15% and $T^*_2$=500 ms) or even by 2 m of subglacial aquifer on soft sediments (w=4% and $T^*_2$ = 250 ms). Nevertheless, reflectors from GPR data beneath the glacier shows aggradational features (Table 1, Fig. 8b), interpreted as sedimentary structures of soft sediments suggesting the presence of a porous aquifer beneath the glacier. The penultimate MRS

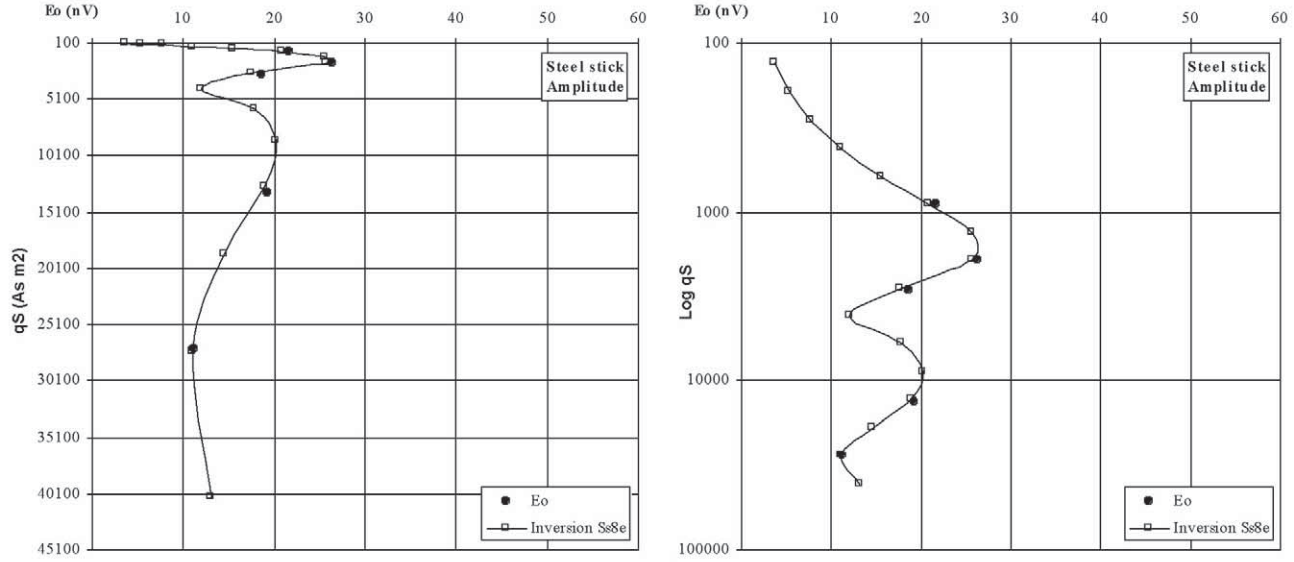


Fig. 8c. Steel stick site data from Table 5c and model from Table 6 following the previous models: Superficial features and crevassed zone on cold-ice with w = 1.3% ($T^*_2$ = 510 ms) between 6.2–8.8 m depth and w = 0.5% between 8.8–14 m depth ($T^*_2$ = 270 ms); temperate-ice layer (CTS and IRH) boundary with w =0.8% between 38.5–46.6 m depth ($T^*_2$ = 90 ms); glacier bottom with w= 1.7% and $T^*_2$ = 600 ms between 73 and 74.5 m depth; subglacial aquifer w =0.7% and $T^*_2$ = 80 ms between 77.5 and 87.5 m depth

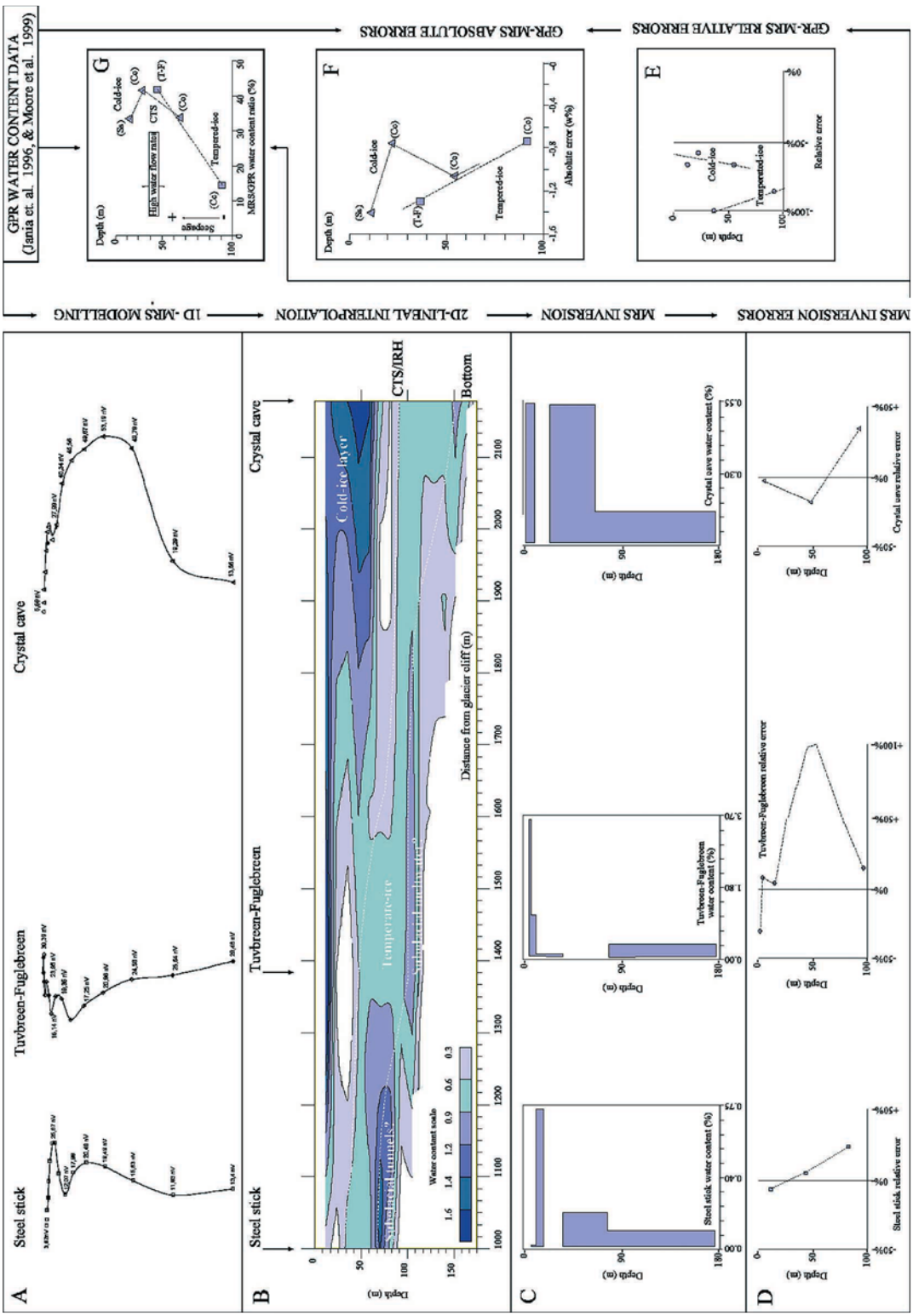


Fig. 9. MRS modelling with GPR data and MRS inversion for Steel Stick site, Tuvbreen-Fuglebreen site and Crystal cave site. Fig. 9a: Data from 1D modelling from Fig. 8. Figure 9b: Two dimension interpolations from previous data, it is possible to distinguish the boundary between cold-ice and the temperate-ice layer and the bottom of the Hansbreen glacier. Figure 9c: MRS Inversion from previous data looking for the smaller relative error; here it is possible to see that Crystal Cave has the most high water content values. Figure 9d: Relative errors between MRS modelled data and inversion, some data shows relative errors of 100% when thin water content layers are not detected individually by MRS. Figure 9e: Relative errors between MRS inverted data and GPR data, all inverted data underestimate more than 50% the GPR water content. Divergent relative error tendencies between cold-ice and temperate-ice layer happen. Figure 9g: Direct comparison between GPR and MRS inverted data is plotted, different ratio trends for cold-ice layer. From that figure it is possible to see that when cold-ice layer is close to the temperate-ice layer the trends of that ratio change to converge. From that ratio different water flow rates and types into ice can be expected. Ss = Steel stick site, Cc = Crystal cave site, T–F = Tuvbreen-Fuglebreen site, CTS = Cold/Temperate transition surface

Table 7. MRS relative errors between model and inversion following Legchenko (2007)

| Glacial zones | Steel stick | | | Tuvbreen-Fuglebreen | | | Crystal cave | | |
|---|---|---|---|---|---|---|---|---|---|
| | Depth | w% | Er% | Depth | w% | Er% | Depth | w% | Er % |
| Cold-ice | | | | 1.0 m | 1.05 | –30.65 | 5 m | 5.25 | –3.33 |
| | | | | 3.5 m | 3.05 | +8.19 | | | |
| | 14 m | 0.5 | –6.35 | 14.3 m | 4.16 | +4.16 | | | |
| CTS? | | | | | | | 54.4 m | 1.5 | –19.8 |
| CTS | 42 m | 0.8 | +5.55 | | | | | | |
| Temperate-ice | 82 m | 0.7 | +24.3 | 36.5 m | 1.25 | +100 | 91 m | 0.7 | +31.7 |
| | | | | 52 m | 0.8 | +100 | | | |
| Glacier bottom | 73 m | | | 95m | 1 | +14.9 | 150 m | | |

Positive values imply that the modelled data overestimates the inverted water content and negative relative errors the opposite. w % = Water content; Er % = Relative errors; CTS = Cold/Temperate surface.

recorded point can be attributed to the CTS/IRH boundary at 40 m depth (Table 1, Fig. 8b). Cold-ice crevassing and moulins are present at shallow depth (< 15 m).

Once the three discrete 1D models have been obtained from quantitative MRS data (Fig. 9a), it is possible to draw a 2D model using a linear extrapolation because the glacier system is roughly layered (Fig. 9b).

## MRS inversion

Since the stacked electromagnetic noise is close to half times the instrumental noise, there is less smoothness of the obtained data and fitting solution is required to improve the accuracy of the inversion (Legchenko 2007). Block inversion is used (Yaramanci & Hertrich 2007), for which only a small number of water content layers are involved, and for that specific software is used (Samovar version 7 from Legchenko 2001 provided with the MRS device). The results are shown in Fig. 9c.

The vertical resolution of the MRS method determines the thickness of the aquifer layer in function of the magnetic field gradient created by the loop. It is high close to the surface, and coarse toward the skin depth (for the Numis device, it is ruled by the Prodiviner data acquisition software from Iris-Instruments). The relative errors between modelled and inverted data can be calculated by the product of the water content (w, in relative percentage) and the thickness (Dz, in metres) of the water content layer (Table 7), because its resolution accuracy is better (Legchenko 2007):

$$Er = (w\Delta z_{inv} - w\Delta z_{mod})/w\Delta z_{mod}.$$

MRS accuracy is also limited because the obtained data is an average of water content assuming a homogeneous aquifer horizontally layered. Nevertheless GPR estimated data from Table 1 is used for that purpose.

The relative errors between model and inversion (Table 7) are plotted in Figure 9d between model and inversion. For the Steel stick site, the errors have a linear trend with depth, where at shallow depths the water content is underestimated, while at deeper depths the water content is overestimated. Random behaviour occurs for the Tuvbreen-Fuglebreen site, where at the central part no water content is present via inversion but does via modelling. Finally the first and last evaluated errors from the Crystal cave site had similarities with the Steel stick error trends, while the middle error data had similar random behaviour like in the Tuvbreen-Fuglebreen site.

Because GPR is limited to obtaining different water content data in vertical at different depths, absolute error can be evaluated only in a few depths. The absolute errors can be evaluated directly comparing the water content from GPR data and the MRS inverted data from the same depth:

$$Ea = MRSw - GPRw;$$

But also in a relative manner:

$$Er' = (MRSw - GPRw)/MRSw$$

Estimated errors from the three studied sites are plotted together in Table 7 and Figure 9e, where in all cases the water content is underestimated at more than 50% with respect to the GPR water content data from Table 4.

Table 8. Type water content (as ratio) between MRS inversion data and GPR data

| Glacial zones | Site | MRS-GPR errors | | | | |
|---|---|---|---|---|---|---|
| | | Depth | Wmrs% | Er% | Ea (w %) | Wratio |
| Cold-ice | Steel stick | 11.4 | 0.7 | –66.6 | –1.4 | 33.33 |
| | Crystal cave | 22.25 | 0.54 | –58.5 | –0.76 | 41.54 |
| | | 54 m | 0.54 | –66.2 | –1.06 | 33.75 |
| CTP/IRH | Tuvbreen-Fuglebreen | 36.25 | 0.54 | ~ –100 | –1.3 | 41.54 |
| Temperate-ice | Crystal cave | 91 m | 0.12 | –85.8 | –0.73 | 14.12 |

Water content data from MRS inversion compared with GPR data, absolute and relative errors. Negative values imply that the MRS inversion data underestimates GPR data from Table 4. Wmrs% = Water content from inverted MRS data; Er% and Ea%= Relative and absolute errors between GPR data and MRS inverted data; Wratio = Water content ratio between MRS inverted data versus GPR reported data.

### Relative and absolute errors

One possibility to explain high differences between inverted MRS data and GPR data (Table 8, Fig. 9e) is that data from Moore et al. (1999) can be too old to compare with the surface NMR survey done in 2009. Nevertheless, that seems not to be the main reason. Direct determinations of water content of other polythermal glaciers (Pettersson 2004) had provided similar values (0.8 +/–0.2%) for temperate-ice just below the cold-ice layer (on the CTS zone). So, similar water content values are possible for the same thermal structures on such glaciers.

From the MRS data, only a few metres are saturated with free water close to the IRH boundary. In all the three studied sites, it was impossible to obtain a model extrapolating the GPR water content to all the temperate-ice layer (see Fig. 7) as is suggested by Jania et al. (1996, p. 63), even when the GPR data shows more or less dense reflections below the IRH. The only explanation for that dichotomy is that some water content might act as bound water (Legchenko com. pers. 2009). In general some of those GPR reflections might come from small water veins separated from seepage (supercooled meltwater). Such water, caught in a low permeability medium ($\sim 10^{-2}$ m per year or less), must have very low relaxation time (<40 ms). Retained water within the ice but still in liquid form, perhaps, is due to impurities altering the pressure melting point (similar features has been reported by Jania et al. 1996, page 63). Such very low decay times of $T^*_2$ are difficult to obtain with the Numis System but further works are in progress in that sense leading by the GMR NMR device from Vista-Clara Inc.

## Discussion

From relative errors (Table 8, Fig. 9e) some direct implications arise: Systematically no positive errors exist. The MRS Numis System inversion data does not show the whole water content within ice (GPR water content data), but only a fraction that can flow, the "free water" with time decays $T_2^* > 40$ ms. Relative errors on the cold-ice layer are quite constant with depth, because relationships between meltwater and water filled cavities (water bodies or englacial channels detected by Moore et al. 1999 in the cold-ice layer) are ought to be constant and climatically dependent. In that sense Moore et al. (1999) found that the thickness of the cold-ice layer decreases across the moulin zones and associated bedrock sills while Jania et al. (1996) using thermistors data close to crevasses found cooling during dry winters and warming during summer by superficial meltwater percolation.

Close to the Glacier surface, high absolute errors (Table 8, Fig. 9f) indicate important water anisotropies at superficial depths (the same was reported by Moore et al. 1999). But such absolute errors diminish with depth, indicating that water amount in englacial conduits are more homogeneous toward the CTS.

Looking at the absolute errors (~water content type differences) from the Crystal cave MRS site (Fig. 9f) it is possible to see a changing behaviour toward the CTS (at 54 m depth, Table 1 and Table 8). For that site, no reflections are present between 50 m and 100 m depth (cold ice, Fig. 8a) from Mariusz Grabiec GPR data, while plenty of reflections are present above and below. The same feature was reported by Moore et al. (1999, page 530), where the highest water content values were found in the temperate-ice. Because relative errors for the temperate-ice layers are larger than their corresponding values for the cold-ice layers (Fig. 9e), high free water content close to CTS should to be there and high "free water" amounts should be present in the CTS. That can also be seen from the ratio between MRS inverted data and GPR data (Table 8 and Fig. 9g), where low values on that ratio ought to also imply a low seepage amount with depth or high free water content.

Absolute errors on temperate-ice layer seems to diminish with depth (Fig. 9f), but in essence no data is available from the GPR survey from Moore et al. (1999) at the same places where MRS data yet available. For the temperate-ice layer only an estimation of the GPR water content has been done (Table 1), nevertheless Hertrich and Walbrecker (2008) using the Numis System found an MRS water content of 1.05±0.5% in the Valais alpine glacier and a GPR water content of about 1.7% (Walbrecker et al. 2008), similar to the Table 1 reported values. In the next future GPR water content data from Hansbreen temperate-ice will be available, then comparing it with MRS data the seepage patterns with depth will be known.

## Conclusions

No convergent results are obtained between MRS and GPR data, basically because both measure different kind of water content within the ice. That conclusion don't agree with Walbrecker et al. (2008) similar work in the Valais alpine glacier, but strong differences between glaciers are probably enough to explain different conclusions about MRS and GPR data. Total water content in ice is obtained from GPR data and only "free water" content in ice is obtained with Numis MRS System data. Combining both data glaciologists, will have a powerful toolkit to be used in englacial and subglacial drainage flow paths exploration. Nevertheless using a more precise NMR device (GMR from Vista-Clara Inc.) is possible to obtain both kind of bound and free water content on ice.

From the MRS results, it is possible to distinguish five water relaxation signal facies for square loops antennas ranging 900 $m^2$ to 14,400 $m^2$:

1) Superficial signals: High amplitudes (>30 nV) and high decay time (>240 ms) to medium decay times are obtained. They are related to superficial runoff, crevasses and moulins.
2) Dry-ice signals: Low (<20 nV) to very low (<10 nV) amplitudes and low decay times are always obtained (<100 ms). They are related to the cold-ice layer, and also to dry temperate-ice.
3) Wet-ice signals: Very high amplitudes (>50 nV) and low to medium relaxation times. They are related to high amounts of "free water" within the Cold/Temperate transition surface.
4) Seepage signal: Low amplitudes (<25 nV) at medium to high pulse moments with short decay times. They are related to seepage within the temperate-ice layer.
5) Subglacial drainage signals: Moderate amplitudes (<30 nV) and very large decay times can be observed, even more than 1 second decay times. To explore those signals, it is convenient to change the window acquisition time to more than 240 ms. If the device is powerful enough, it will be also convenient to change the duration of the excitation pulse to more than 40 ms. It seems to be related to some of the possible subglacial meltwater drainage, via porous media, tunnels or sheet flow. The absence of such water signal facies means that neither the glacier bottom nor the bedrock has been reached.

The multiple loop size configurations used for each surveyed site provided satisfactory results. Such a methodology makes it easy to model a synthetic sounding by adding the best data quality of the single soundings.

## Acknowledgements

I wish to thank the Polish Academy of Sciences, and especially Piotr Glowacki from the Polar and Marine Research Department of the Institute of Geophysics for granting the Hornsund stay for the NMR project. Many thanks to Sebastian Sikora and his team at the 32st expedition on the Polish Polar Station from Isbjörnhamma Bay in Hornsund fjord for their hospitality. I wish also to thank Jacek Jania and his team from the Silesia University in field assistance, technical support and scientific discussions. Also thanks to Doug Benn from the UNIS at Longyearbyen and his field assistant for their help and experience. To Olivier Hengesch from the University of Luxemburg for his great company in Hornsund and in Longyearbyen. To Dariusz Ignatiuk to invite me at the Zieleniec 2010 workshop and to carry on the 2012 magnetic susceptibility measurements in Hornsund. To Mariusz Grabiec for his scientific data and very pleasant discussions in Zieleniec. To Wojciech Dobiński for his great company and to Krzysztof Migala for his kindness and stance in the city of Wrocław in January 2010. Thank you to Rafik Soltani for his help and MRS calculations, also to Anatoly Legchenko for his constructive comments on the MRS results. To Juan Plata, Marian Hertrich and Marian Lüthi I wish to thank you all the comments on the first version of this paper and their suggestions to improve it. And last, but not least, many thanks to all persons who directly or indirectly helped to make the project possible.

## References

Behroozmand A., Auken E., Fiandaca G. & Christiansen A.V., 2012. Improvement in MRS parameter estimation by joint and lateral constrained inversion of MRS and TEM data. Geophysics 77(4): WB191-WB200.

Benn D., Gulley J., Luckman A., Adamek A. & Glowaki P., 2009. Englacial drainage systems formed by hydrologically driven crevasse propagation. Journal of Glaciology 55(191): 513–523.

Bennett M.R. & Glasser N.F., 2009. Glacial Geology. 2nd ed. Willey-Blackwell, Singapore.

Bernard J., 2007. Instruments and field work to measure a Magnetic Resonance Sounding. Boletin Geologico y Minero 118(3): 459–472.

Hertrich M. & Walbrecker J., 2008. The potential of surface-NMR to image water in permafrost and glacier ice. Geophysical Research Abstracts, V10, SRef-ID: 1607–7962/gra/EGU2008-A–06663.

Hertrich M., 2008. Imagining of groundwater with nuclear magnetic resonance. Nuclear Magnetic Resonance Spectroscopy 53: 227–248.

Jania J., Mochnacki D. & Gadek B. 1996. The thermal structure of Hansbreen, a tidewater glacier in southern Spitsbergen, Svalbard. Polar Research 15(1): 53–66.

Kostrzewski A. & Zwolinski Zb. (eds.), 2007. Geodiversity of polar landforms. Landform Analysis 5: 1–220.

Legchenko A. & Shushakov O.A., 1998. Inversion of surface NMR data. Geophysics 63(1): 75–84.

Legchenko A. 2007. MRS measurements and inversion in presence of EM noise. Boletin Geologico y Minero 118(3): 489–508.

Menzies J., 1995a. The dynamics of ice flow. In: J.Menzies (ed.), Modern glacial environments, Butterworth-Heinemann Ltd, Oxford, 1: 139–196.

Menzies J., 1995b. Hydrology of glaciers. In: J.Menzies (ed.), Modern glacial environments, Butterworth-Heinemann Ltd, Oxford, 1: 197–239.

Moore J.C., Pälli A., Ludwig F., Blatter H., Jania J., Gadek B., Glowacki P., Mochnacki D. & Isaksson E., 1999. High-resolution hydrothermal structure of Hansbreen, Spitsbergen, mapped by ground-penetrating radar. Journal of Glaciology 45(151): 524–532.

Oerlemans J., Jania J. & Kolondra L., 2011. Application of a minimal glacier model to Hansbreen, Svalbard. The Cryosphere 5: 1–11.

Pälli A. 2003. Polythermal glaciers studies in Svalbard determined by ground-penetrating radar. PhD thesis. Department of Geosciences, Oulu University.

Petterson R. 2004. Dynamics of the cold surface layer of polythermal Storglaciaren, Sweden. PhD thesis. Department of Physical Geography and Quaternary Geology, Stockholm University.

Plata J.L. & Rubio F.M., 2007. Basic theory of the Magnetic Resonance Sounding: Method. Boletín Geológico y Minero 118(3): 441–458.

Walbrecker J., Hertrich M. & van der Kruk J., 2008. Water content determination on the Rhone glacier (Valais, Switzerland) using sample-scale-NMR, surface-NMR and GPR methods. DGG-Jahrestagung, Freiberg.

Yaramanci U. & Hertrich M., 2007. Inversion of Magnetic Resonance Sounding data. Boletin Geologico y Minero 118(3): 473–488.